

Role of Hydrogen Bonds in Benzimidazole-Based Organic Magnetic Materials: Crystal Scaffolding or Exchange Linkers?

Jacqueline R. Ferrer,[†] Paul M. Lahti,^{*,†} Clifford George,[‡] Patricia Oliete,[§] Michel Julier,[§] and Fernando Palacio[§]

Department of Chemistry, University of Massachusetts, Amherst, Massachusetts 01003,
Laboratory for the Structure of Matter, Naval Research Laboratory, Washington, DC, 20375,
and Instituto de Ciencia de Materiales de Aragón, CSIC Universidad de Zaragoza,
50009 Zaragoza, Spain

Received April 12, 2001

The highly stable nitroxide radicals 5(6)-chloro-2-(*N*-*tert*-butyl-*N*-aminoxyl)benzimidazole (**4**) and 5,6-dimethyl-2-(*N*-*tert*-butyl-*N*-aminoxyl)benzimidazole (**5**) were synthesized and characterized by electron spin resonance spectroscopy, crystallography, and magnetic susceptibility. Both crystallize as dimeric pairs with N–H hydrogen bond donors and N–O acceptors. This behavior contrasts to that of analogous 2-(*N*-*tert*-butyl-*N*-aminoxyl)benzimidazole (**3**), which forms hydrogen-bonded chains (Ferrer, J. R.; Lahti, P. M.; George, C.; Antorrena, G.; Palacio, F. *Chem. Mater.* **1999**, *11*, 2205–2210). Susceptibility analysis shows dimeric antiferromagnetic exchange coupling with $J/k = -22$ K for **4** and -24 K for **5**. Density functional theory (DFT) computations support a N–O to N–O throughspace antiferromagnetic exchange mechanism as the major contributor to the overall magnetic behavior of **4** and **5**. A spin–polarization exchange coupling mechanism involving a cyclic exchange path using the –N–H···O–N hydrogen bonds in the dimers is expected to yield ferromagnetic coupling between dimers, in contradiction to the experimental and DFT results. The hydrogen bonds in **4** and **5** thus act more as structural scaffolding to hold the radicals in proximity rather than as electronic exchange linkers.

Introduction

Since the initial report that the β phase of the organic stable radical *p*-nitrophenyl nitronyl nitroxide (**1**) exhibits ferromagnetic ordering at 0.65 K,¹ considerable effort has been put into studies of the structure–property relationships between crystal packing and bulk exchange between unpaired electrons. Organic systems are of considerable interest because of possibilities to control exchange pathways by hydrogen bonding or coordination between organic open-shell molecules and paramagnetic ions.² Although most purely organic systems have ordering temperatures well below the boiling point of liquid helium (4 K), the recent report of the β -phase soft ferromagnet 4-cyano-3,4,5,6-tetrafluoro-

rophenyldithiadiazolyl³ (**2**; $T_c = 36$ K) raises the prospects of much higher ordering temperatures for organic systems.

Hydrogen bonding in molecular recognition and crystal engineering is fundamental to chemistry and has played a role in the design strategies⁴ to make purely organic magnetic materials. We have previously reported that 2-(*N*-*tert*-butyl-*N*-aminoxyl)benzimidazole^{5,6} (**3**) exhibits antiferromagnetic exchange in the solid state and shows magnetic susceptibility behavior that

(3) (a) Palacio, F.; Antorrena, G.; Castro, M.; Burriel, R.; Rawson, J.; Smith, J. N. B.; Bricklebank, N.; Novoa, J.; Ritter, C. *Phys. Rev. Lett.* **1997**, *79*, 2336–2339. (b) Palacio, F.; Castro, M.; Antorrena, G.; Burriel, R.; Ritter, C.; Bricklebank, N.; Rawson, J.; Smith, J. N. B. *Mol. Cryst. Liq. Cryst. Sci. Technol., Sect. A* **1997**, *306*, 293–300.

(4) (a) Sugawara, T.; Matsushita, M. M.; Izuoka, A.; Wada, N.; Takeda, N.; Ishikawa, M. *J. Chem. Soc., Chem. Commun.* **1994**, 1723. (b) Sugawara, T.; Izuoka, A. *Mol. Cryst. Liq. Cryst. Sci. Technol., Sect. A* **1997**, *305*, 41–54. (c) Sugawara, T.; Nakazaki, J.; Matsushita, M. M. In *Magnetic Properties of Organic Materials*; Lahti, P. M., Ed.; Marcel Dekker: New York, 1999; Chapter 26, pp 540–545. (d) Cirujeda, J.; Ochando, L. E.; Amigó, J. M.; Rovira, C.; Rius, J.; Veciana, J. *Angew. Chem., Int. Ed. Engl.* **1995**, *34*, 55. (e) Cirujeda, J.; Hernández-Gasió, E.; Panthou, F. L.-F.; Laugier, J.; Mas, M.; Molins, E.; Rovira, C.; Novoa, J. J.; Rey, P.; Veciana, J. *Mol. Cryst. Liq. Cryst.* **1995**, *271*, 1. (f) Cirujeda, J.; Hernández-Gasió, E.; Rovira, C.; Stanger, J.-L.; Turek, P.; Veciana, J. *J. Mater. Chem.* **1995**, *5*, 243–252. (g) Zhang, J.; Wang, R.; Baumgarten, M. *Mol. Cryst. Liq. Cryst.* **1997**, *306*, 705–710.

(5) (a) Ferrer, J. R.; Lahti, P. M.; George, C.; Antorrena, G.; Palacio, F. *Chem. Mater.* **1999**, *11*, 2205–2210. (b) Lahti, P. M.; Esat, B.; Ferrer, J. R.; Liu, Y.; Marby, K. A.; Xie, C.; George, C.; Antorrena, G.; Palacio, F. *Mol. Cryst. Liq. Cryst. Sci. Technol., Sect. A* **1999**, *334*, 285–294.

(6) Mathias, L. J.; Overberger, C. G. *J. Org. Chem.* **1978**, *43*, 3518–3526.

[†] University of Massachusetts.

[‡] Naval Research Laboratory.

[§] Universidad de Zaragoza.

(1) Takahashi, M.; Turek, P.; Nakazawa, Y.; Tamura, M.; Nozawa, K.; Shiomi, D.; Ishikawa, M.; Kinoshita, M. *Phys. Rev. Lett.* **1991**, *67*, 746–748.

(2) (a) Kahn, O. *Molecular Magnetism*; VCH: New York, 1993. (b) Lahti, P. M. *Magnetic Properties of Organic Materials*; Marcel Dekker: New York, 1999. (c) Gatteschi, D.; Kahn, O.; Miller, J. S.; Palacio, F. *Magnetic Molecular Materials*; Kluwer Academic Publishers: Dordrecht, The Netherlands, 1991. (d) Iwamura, H.; Miller, J. S., Eds. *Mol. Cryst. Liq. Cryst.* **1993**, *232–233*, 1ff. (e) Miller, J. S., Epstein, A., Eds. *Mol. Cryst. Liq. Cryst.* **1995**, *270–271*, 1ff. (f) *Molecule-Based Magnetic Materials. Theory, Techniques, and Applications*; Turnbull, M. M., Sugimoto, T., Thompson, L. K., Eds.; American Chemical Society: Washington, DC, 1996. (g) Itoh, K.; Miller, J. S.; Takui, T., Eds. *Mol. Cryst. Liq. Cryst.* **1995**, *305–306*, 1ff. (h) Kahn, O., Ed. *Mol. Cryst. Liq. Cryst. Sci. Technol., Sect. A* **1999**, *334–335*, 1ff.

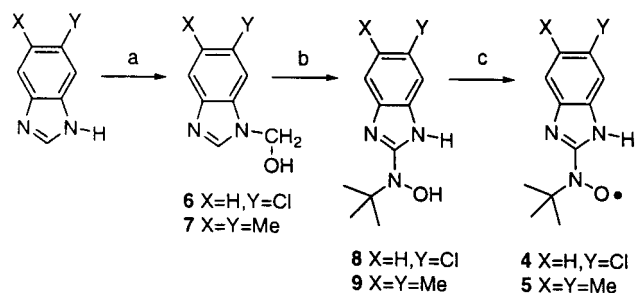
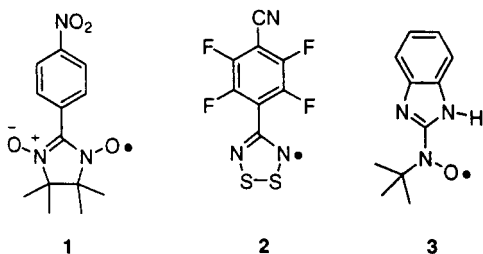


Figure 1. Synthesis of radicals **4** and **5**: (a) MeOH/paraform; (b) *n*-BuLi/hexanes/ -75°C and then *t*-Bu-N=O; (c) PbO₂/CHCl₃/rt.

is consistent with the extended hydrogen-bonded stacking of its crystal structure. We aimed to probe the effect of substitution upon crystal packing and magnetic properties of benzimidazole-2-*tert*-butyl nitroxides. In this paper, we report the synthesis, crystallography, and magnetic behavior of 5(6)-chloro-2-(*N*-*tert*-butyl-*N*-aminoxyl)benzimidazole (**4**) and 5,6-dimethyl-2-(*N*-*tert*-butyl-*N*-aminoxyl)benzimidazole (**5**).



Results

Synthesis and Characterization. Figure 1 details the syntheses of **4** and **5**. 5(6)-Chlorobenzimidazole was prepared from 4-chloro-1,2-diaminobenzene and formic acid using the method of Mathias and Overberger.⁶ 5,6-Dimethylbenzimidazole was made by the method of Varma et al.⁷ from 1,2-diamino-4,5-dimethylbenzene. The benzimidazoles were converted to *N*-hydroxymethyl derivatives **6** and **7** by treatment with paraformaldehyde. Treatment of **6** and **7** with *n*-butyllithium gave the corresponding carbanions at the 2 position because of the directing effect of the hydroxymethyl group. Treatment of the anions with 2-methyl-2-nitrosopropane⁸ gave hydroxylamines **8** and **9**. Oxidation of the hydroxylamines in chloroform with lead dioxide gave corresponding nitroxides **4** and **5** as red solids that are stable for months in air.

The electron spin resonance (ESR) spectra of **4** and **5** were obtained at room temperature in benzene. Hyperfine coupling constants (hfc) were obtained by line-shape analysis using the WINSIM program of Duling⁹ and are listed in Table 1. The table also lists the computed hfc for **4** and **5** obtained using Gaussian 98¹⁰ on a Silicon Graphics Octane computer at the pure density functional Becke–Lee–Yang–Parr^{11a,b} (BLYP) and hybrid B3LYP^{11c} levels of theory using the cc-pVDZ¹² basis set. Molecular geometries were taken

directly from the crystallographic analyses. The BLYP density functional method gives hfc that are in good agreement with experimental values for nitroxide-based radicals.¹³ The B3LYP results were not greatly different from the BLYP results and so are summarized only in the Supporting Information.

Crystallography. Single crystals of **4** and **5** were subjected to X-ray analysis and the data analyzed using SHELXTL97.¹⁴ Figures 2 and 3 show various views of the crystal structures and packing. The figure shows N–H···O–N hydrogen bonds in the lattice as dashed lines; only the hydrogen atoms involved in this interaction are explicitly shown. The estimated N–H···O bond distances for **4** and **5** are both about 1.8 Å if one assumes that $r(\text{N–H})$ is 1.1 Å,^{14b} and the N–H···O angles deviate somewhat from linearity. The nitroxide group itself is essentially planar in both structures. The nitroxide N–O bonds are oriented syn to the N–H bond direction and are highly coplanar with the benzimidazole rings in both cases. Various computations show the crystallographic syn conformer to be favored over a putative anti conformer, in which the nitroxide group is rotated by 180° relative to the syn conformer.

Tables 2 and 3 give space group parameters and crystallographic coordinates for **4** and **5**, respectively. Table 4 gives comparative geometric parameters for **4** and **5** and their basic dimeric units in the solid state. Further details may be found in the Supporting Information. Full tables of atomic coordinates, bond distances, bond angles, anisotropic thermal parameters, and additional data collection and refinement parameters will be deposited with the Cambridge Structural Database.¹⁵

Magnetic Susceptibility. Magnetization measurements for **4** and **5** were carried out on 13.4 and 16.8 mg samples, respectively, at an external magnetic field of 1 T over a temperature range of 1.8–300 K. The magnetic behavior was modeled by considering the molecules as antiferromagnetically (AFM) coupled dimers, where the susceptibility χ per mole of dimers (assuming all spin $S = 1/2$ molecules) obeys the Bleaney–Bowers equation.¹⁶ Details are given in the Supporting Information.

The experimental data and the fitted magnetization curves for **4** and **5** are given in Figures 4 and 5. The

(10) Frisch, M. J.; Trucks, G. W.; Schlegel, H. B.; Gill, P. M. W.; Johnson, B. G.; Robb, M. A.; Cheeseman, J. R.; Keith, T.; Petersson, G. A.; Montgomery, J. A.; Raghavachari, K.; Al-Laham, M. A.; Zakrzewski, V. G.; Ortiz, J. V.; Foresman, J. B.; Cioslowski, J.; Stefanov, B. B.; Nanayakkara, A.; Challacombe, M.; Peng, C. Y.; Ayala, P. Y.; Chen, W.; Wong, M. W.; Andres, J. L.; Replogle, E. S.; Gomperts, R.; Martin, R. L.; Fox, D. J.; Binkley, J. S.; Defrees, D. J.; Baker, J.; Stewart, J. P.; Head-Gordon, M.; Gonzalez, C.; Pople, J. A. *Gaussian 98*, Revision A.3; Gaussian Inc.: Pittsburgh, PA, 1998.

(11) (a) Becke, A. D. *Phys. Rev. A* **1988**, *38*, 3098–3100. (b) Lee, C.; Yang, W.; Parr, R. G. *Phys. Rev. B* **1988**, *37*, 785–789. (c) Becke, A. D. *J. Chem. Phys.* **1993**, *98*, 5648–5652.

(12) Woon, D. E.; Dunning, T. H., Jr. *J. Chem. Phys.* **1993**, *98*, 1358–1371.

(13) Novoa, J. J.; Mota, F.; Veciana, J.; Cirujeda, J. *Mol. Cryst. Liq. Cryst.* **1995**, *271*, 79–90.

(14) (a) Sheldrick, G. M. *SHELXTL97 Program for the Refinement of Crystal Structures*; University of Göttingen: Göttingen, Germany, 1997. (b) Hydrogen atom crystallographic coordinates in this paper are values obtained by a riding model without correction. Details are given in the Supporting Information.

(15) Cambridge Structural Database, version 5.19 (April 2000), from the Cambridge Crystallographic Data Centre, Cambridge CB2 1EZ, UK.

(16) Bleaney, B.; Bowers, K. D. *Proc. R. Soc. London A* **1952**, 214.

(7) (a) Varma, R. S.; Kapoor, A.; Ellis, G. *Eur. J. Med. Chem. Chim. Therapeutica* **1980**, *6*, 536–538. (b) Varma, R. S. *J. Indian Chem. Soc.* **1977**, *727*–728.

(8) Stowell, J. C. *J. Org. Chem.* **1971**, *36*, 3055.

(9) Duling, D. R. *J. Magn. Reson.* **1994**, *B104*, 105–110.

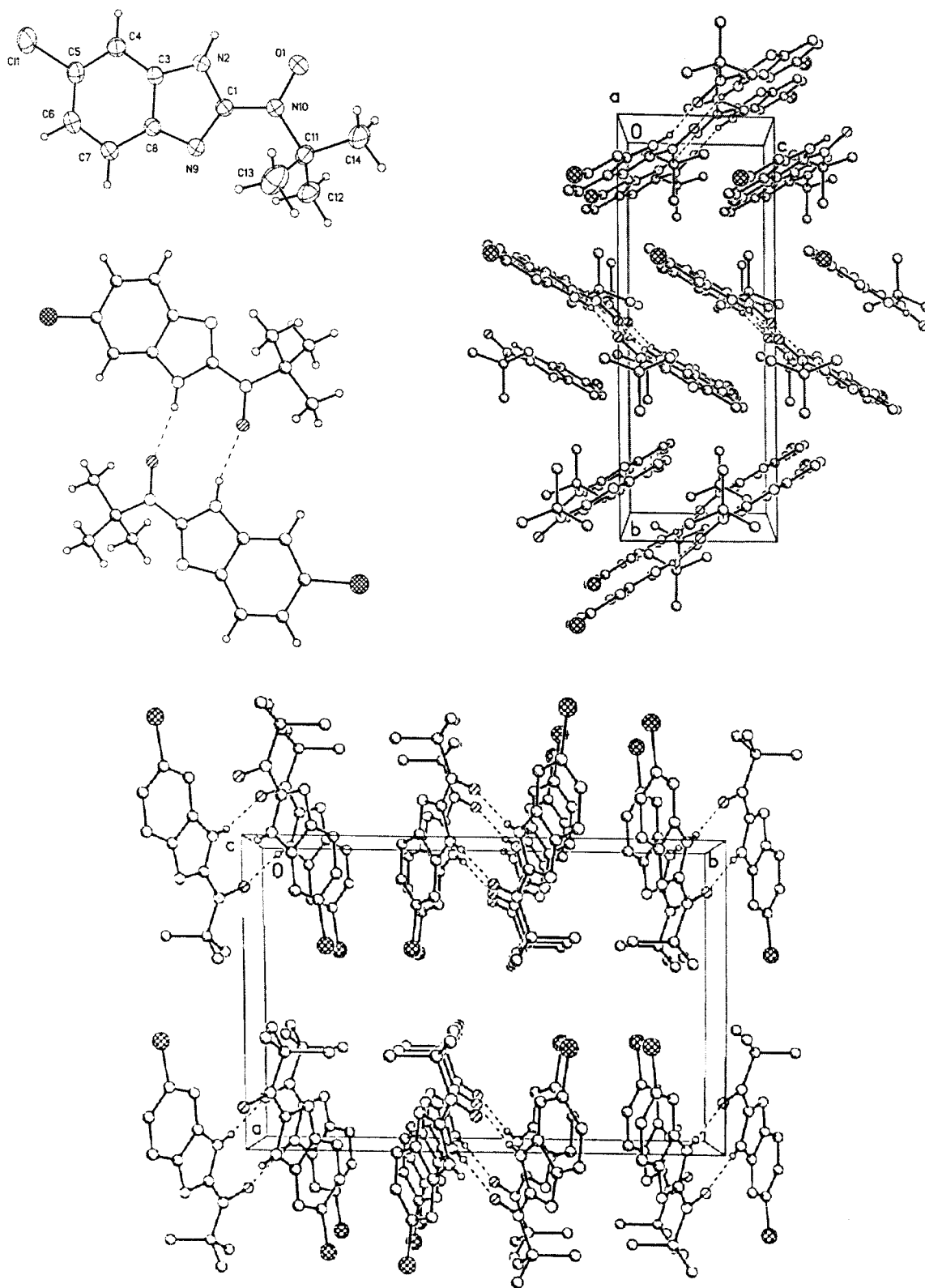


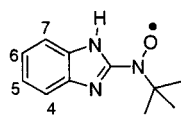
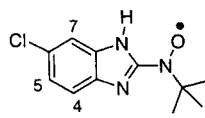
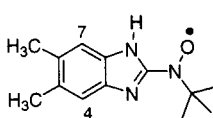
Figure 2. ORTEP diagram of radical **4**, ORTEP diagram of one dimeric pair, and crystal packing views along the *a* and *c* axes. Dashed lines show hydrogen bonds between dimer pairs.

data reflect the correction for diamagnetic contributions, which were obtained experimentally using an empty sample holder, and sample diamagnetism estimated by Pascal's constants. For **4**, the fitted dimeric AFM exchange constant $J/k = -21.9$ K; for **5**, $J/k = -24.0$ K. The data fit shows some isolated paramagnetic spin sites: $<0.4\%$ in **4** and about 4% in **5**.

Discussion

The ESR spectra of **4** and **5** show their spin-density distributions to be very similarly to that of the previously described analogue, **3**. Assuming the McConnell relationship to hold true with a proportionality constant of -22 G to convert spin-density populations to hfc, the

Table 1. Experimental and Computed hfc for 3–5

Compound	Experimental hfc	Computed hfc ^b
	$a(\underline{\text{N-O}}) = 10.16 \text{ G}^a$ $a(\underline{\text{N-H}}) = 0.77^a$ $a(=\text{N-}) = 2.13^a$ $a(\underline{\text{N-H}}, \text{H4-7}) = 0.88, 0.51,$ $0.37, 0.21,$ 0.11^a	$a(\underline{\text{N-O}}) = 7.14 \text{ G}$ $a(\underline{\text{N-H}}) = 0.30$ $a(=\text{N-}) = 2.30$ $a(\text{H4,7}) = (-)0.73, (+)0.07$ $a(\text{H5,6}) = (-)0.04, (-)1.02$ $a(\underline{\text{N-H}}) = (-)0.61$
	$a(\underline{\text{N-O}}) = 10.0 \text{ G}$ $a(\underline{\text{N-H}}) = 0.44$ $a(=\text{N-}) = 2.12$ $a(\underline{\text{N-H}}, \text{H4,5,7}) = 0.85, 0.79,$ $0.59, 0.45$	$a(\underline{\text{N-O}}) = 6.85 \text{ G}$ $a(\underline{\text{N-H}}) = 0.29$ $a(=\text{N-}) = 2.31$ $a(\text{H4,7}) = (-)0.86, (+)0.11$ $a(\text{H5}) = (-)0.07$ $a(\underline{\text{N-H}}) = (-)0.58$
	$a(\underline{\text{N-O}}) = 10.25 \text{ G}$ $a(\underline{\text{N-H}}) = 0.38$ $a(=\text{N-}) = 2.17$ $a(\underline{\text{N-H}}, \text{H4;7,Me}) = 0.19 \text{ (1H)}$ $0.39\text{-}0.53 \text{ (5 H)}$ $1.15\text{-}1.31 \text{ (3 H)}$	$a(\underline{\text{N-O}}) = 7.05 \text{ G}$ $a(\underline{\text{N-H}}) = 0.31$ $a(=\text{N-}) = 2.25$ $a(\text{H4,7}) = (-)0.66, (+)0.14$ $a(\underline{\text{N-H}}) = (-)0.61$ $a(\text{CH}_3) = (\pm)0.03\text{-}1.71$

^a Reference 5. hfc for **4** were refit with the addition of $a(\text{N-H})$ as a variable. The changes in the hfc were less than experimental uncertainty. All hfc fit using program WINSIM (ref 9). ^b Computed at crystallographic geometries using the BLYP/cc-pVDZ level of theory. Computed hfc of the aryl-methyl groups in compound **6** are geometry dependent. See the Supporting Information for geometries used.

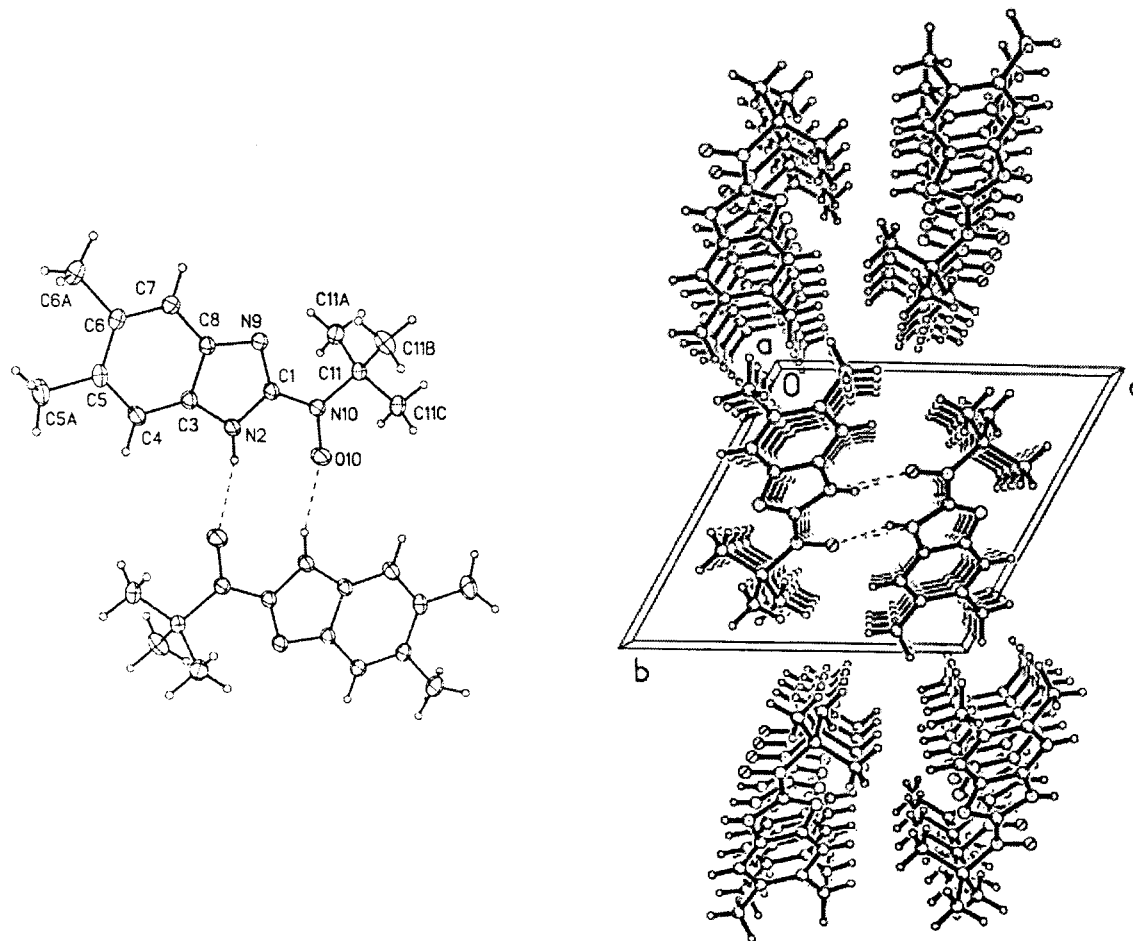


Figure 3. ORTEP diagram of one dimeric pair of radical **5** and crystal packing along the *a* axis. Dashed lines show hydrogen bonds between dimer pairs.

percentage spin density on the nitroxide nitrogen is ~45% for both **4** and **5**. The experimental hfc of 10.2 G

for the nitroxide *nitrogen* of **3** corresponds to essentially the same spin density, 46%. BLYP/cc-pVDZ computa-

Table 2. Atomic Coordinates ($\times 10^{-4}$) and Equivalent Isotropic Displacement Parameters ($\text{\AA}^2 \times 10^3$) for Radical 4^a

	<i>x</i>	<i>y</i>	<i>z</i>	<i>U</i> (eq)
Cl(1)	-3456(1)	6618(1)	7300(2)	117(1)
C(1)	1139(3)	5901(2)	3021(5)	53(1)
N(2)	-35(2)	5716(2)	2727(4)	59(1)
C(3)	-578(3)	6045(2)	4382(5)	55(1)
C(4)	-1765(3)	6087(2)	4849(6)	70(1)
C(5)	-1988(3)	6500(2)	6658(6)	72(1)
C(6)	-1096(3)	6851(2)	7938(6)	71(1)
C(7)	76(3)	6813(2)	7460(5)	67(1)
C(8)	339(3)	6408(2)	5632(5)	56(1)
N(9)	1418(2)	6313(2)	4737(4)	59(1)
N(10)	1922(2)	5666(2)	1547(4)	58(1)
O(1)	1507(2)	5191(2)	121(4)	85(1)
C(11)	3187(3)	5953(2)	1493(5)	61(1)
C(12)	3920(3)	5628(3)	3371(6)	88(1)
C(13)	3189(4)	6839(2)	1510(9)	111(2)
C(14)	3648(4)	5665(4)	-539(6)	110(2)
H(2)	-330(30)	5480(20)	1660(60)	80

^a Space group $P2_1/c$ ($Z = 4$); $a = 11.224(1)$, $b = 17.100(1)$, and $c = 6.336(1)$ \AA; $\beta = 94.04^\circ$. H(2) is the N–H hydrogen (other hydrogen atom coordinates are listed in the Supporting Information, Table S5A); see ref 14b.

Table 3. Atomic Coordinates ($\times 10^{-4}$) and Equivalent Isotropic Displacement Parameters ($\text{\AA}^2 \times 10^3$) for Radical 5^a

	<i>x</i>	<i>y</i>	<i>z</i>	<i>U</i> (eq)
C(1)	1787(4)	5195(2)	3016(2)	46(1)
N(2)	2209(3)	4415(2)	3622(2)	52(1)
C(3)	3687(4)	3561(2)	2939(2)	46(1)
C(4)	4725(4)	2568(2)	3104(2)	56(1)
C(5)	6167(4)	1886(2)	2239(2)	54(1)
C(5A)	7334(5)	805(3)	2408(3)	79(1)
C(6)	6541(4)	2198(2)	1200(2)	49(1)
C(6A)	8126(4)	1452(3)	256(3)	70(1)
C(7)	5475(4)	3186(2)	1046(2)	51(1)
C(8)	4051(4)	3895(2)	1928(2)	44(1)
N(9)	2838(3)	4936(2)	1994(2)	50(1)
N(10)	350(3)	6174(2)	3505(2)	50(1)
O(10)	-587(4)	6222(2)	4476(2)	81(1)
C(11)	-51(4)	7226(2)	3038(2)	46(1)
C(11C)	-1661(5)	8105(3)	3879(3)	69(1)
C(11B)	-1158(5)	6443(3)	1568(2)	73(1)
C(11A)	2227(4)	8154(3)	3271(3)	65(1)
H(2)	1640(50)	4450(30)	4280(30)	80

^a Space group $P\bar{1}$ ($Z = 2$); $a = 5.955(1)$, $b = 10.888(1)$, and $c = 11.490(1)$ \AA; $\alpha = 117.99(1)^\circ$, $\beta = 96.06(1)^\circ$, and $\gamma = 96.48(1)^\circ$. H(2) is the N–H hydrogen (other hydrogen atom coordinates are listed in the Supporting Information, Table S5B); see ref 14b.

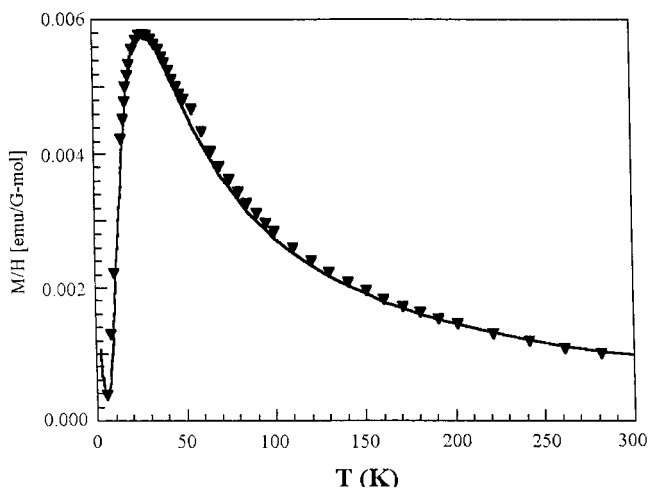
tions give the percent spin densities on the nitrogen and oxygen of the nitroxide units of **3–5** to be 32.4 and 46.3%, 33.6 and 51.0%, and 34.3 and 50.1%, respectively. Both BLYP and B3LYP methods (Supporting Information) underestimate the hfc on the nitroxide nitrogen relative to the experiment. Still, the similarities of both experimental hfc and computed spin densities for **3–5** reinforce the notion that all of the benzimidazole-2-*tert*-butyl nitroxides are very similar in terms of spin-density distributions.

In the crystal structures of **3–5**, the nitroxide N–O bond is aligned parallel to the N–H bond, presumably because of the favorable local dipole alignment in this conformation. The nitroxide N–O unit and the benzimidazole ring are highly coplanar in all three cases, with a range of torsional angles of 8.7, 9.2, and 3.4° in **3–5**, respectively. Radical **3** has previously been shown⁵ to form hydrogen-bonded chains between canted stacks of radicals, an Etter C(4) chain motif¹⁷ (Chart 1)

Table 4. Comparison of Selected Crystallographic Parameters for Radicals 4 and 5

	4	5
$\angle[\text{ON–BIm}]$ torsion ^a	9.2°	3.4°
$r[\text{N–O}]$	1.278 \AA	1.280 \AA
$r[\text{ON–BIm}]$	1.386	1.389
$r[\text{C}(2)–\text{N}(1)]$	1.355	1.354
$r[\text{C}(2)=\text{N}(3)]$	1.315	1.317
<hr/>		
	4 dimer	5 dimer
$r[\text{N–H}\cdots\text{O–N}]^b$	2.03 \AA (1.79 \AA)	2.01 \AA (1.78 \AA)
$r[\text{N–O}\cdots\text{O–N}]$	3.438	3.503
$r[\text{N(H)}\cdots\text{O–N}]^c$	2.823	2.812
$\angle[\text{N–H}\cdots\text{O}]^d$	158.1° (154.9°)	157.7° (154.6°)
<hr/>		
	4 stack	5 stack
plane-to-plane stack distance ^e	3.5 \AA	3.4 \AA
$r[\text{N–O}\cdots\text{O–N}]$	6.34 (<i>c</i> axis)	5.96 (<i>a</i> axis)

^a BIm = benzimidazole ring. Standard numbering used for atoms in the BIm ring measurements. ^b Distance using the uncorrected, riding model coordinates^{14b} for the N–H hydrogen atom; the distance in parentheses assumes that $r[\text{N–H}] = 1.10$ \AA. ^c Distance from the imidazole nitrogen to the nitroxide oxygen in the dimer. ^d Angle using uncorrected hydrogen atom positions from the riding model,^{14b} given in the Supporting Information; the angle in parentheses assumes that $r[\text{N–H}] = 1.10$ \AA. ^e Perpendicular plane-to-plane distance between benzimidazole rings.

**Figure 4.** Plot of magnetization versus temperature for radical **4**. Triangles are experimental data points; the solid curve is based on eq 2 in the text.

involving N–H as a hydrogen bond donor and =N– as an acceptor. By comparison, both **4** and **5** show dimeric pairing of the radicals, an $R_2^2(10)$ ring motif with an N–H donor and an O–N acceptor. This difference correlates with the different appearances of the N–H stretching region of **3** by comparison to those of **4** and **5**. Compound **3** shows a broad N–H stretching absorption that mostly overlays the 3100–2900 cm^{-1} C–H stretching region; this band is shifted to 2310 cm^{-1} by deuteration of the N–H bond. Compounds **4** and **5** both show relatively sharp, well-defined N–H stretches at about 3300 cm^{-1} , well separated from the C–H stretching regions.

The dimers of **4** form canted stacks along the crystallographic *c* axis with a stacking distance of 3.5 \AA between the planes of the benzimidazole rings. Radical

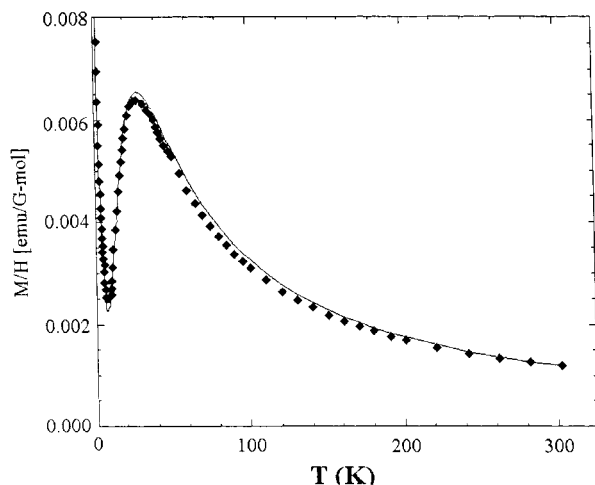


Figure 5. Plot of magnetization versus temperature for radical **5**. Diamonds are experimental data points; the solid curve is based on eq 2 in the text.

4 also exhibits a ribbonlike motif connecting the dimeric stacks, because of herringbone “T” interactions between the C–H bonds at C6 and C7 of one benzimidazole ring and the π cloud of another (Chart 1 and Figure 2, bottom representation). Radical **5** shows only canted stacking of the dimers along the crystallographic *a* axis (Figure 3), with a plane-to-plane distance between rings of 3.4 Å. The 5,6-dimethyl substitution in **5** does not leave two adjacent C–H bonds to form a herringbone “T” interaction like those in **3** and **4**. The series **3–5** represents a monotonic decrease in the unit cell complexity—with *Z* = 8, 4, and 2, respectively—as the herringbone interactions change in the series.

It is not clear why the substitution in **4** and **5** causes dimerization to be favored over the hydrogen-bonded chains in the less-substituted system **3**. A computerized search of the Cambridge Structural Database showed very few examples¹⁸ of hydrogen-bonded dimers involving an imidazole N–H group with either a –C–O group or a –N–O unit directly attached at the 2 position. Extended chains of hydrogen bonding are more common. One analogue, 2-(hydroxymethyl)benzimidazole, forms^{18a} dimers between the imidazole N–H and the hydroxymethyl C–O with a geometry very similar to those of **4** and **5**, save for some additional hydrogen bonding involving the OH group. Possibly, the disruption of linear herringbone interactions in **4** and **5** relative to **3** is just sufficient in these cases to allow the geometrically well-matched dimer formation to occur, whereas in **3** the simultaneous formation of hydrogen-bonded chains, good π stacking, and linear herringbone formation lead to a more extended packing motif. This is a hypothesis that is difficult to prove until further information is available about structural effects on packing of these systems.

The dimers in **4** and **5** can be considered as having a large nitroxide α spin exchange linked by the spin-polarized β spin density on the hydrogen of an N–H group, which in turn is connected to the α spin on the nitrogen of the N–H group (Chart 2). This path, which

follows the closest atomic contacts between the molecules of the dimer, would result in the overall FM exchange between the nitroxide units of the dimer, assuming that the hydrogen bond is an effective exchange linker. Various studies have discussed the possibility of hydrogen bonds as electronic exchange linkers.⁴ However, the hydrogen bonds also could act only as molecular scaffolding to hold the radicals in a well-defined geometry, without being a major contributor to the intermolecular electronic spin exchange (Chart 2). In the latter case, the main exchange interaction would be a direct throughspace interaction between the nitroxides. In the geometry of the dimer, this would tend to favor AFM behavior, because the nitroxide N–O orbitals are not orthogonal.¹⁹ The experimental magnetization results support this second model for our systems, given the observed strong AFM exchange couplings.

To compare these two models further, we studied the exchange coupling in a hydrogen-bonded dimer model by density functional theory (DFT). Both the pure BLYP and hybrid B3LYP functionals were used to study a model dimer for **4** and **5** consisting of an imidazole ring and an H–NO– unit placed in the appropriate geometric relationship based on the crystal structure. Because the experimental ESR spectra show that the large majority of spin density remains in the nitroxide groups, this truncation of the molecular structure should not appreciably alter the spin-density distribution in the model relative to the experiments and still incorporates the main structural features of the Etter R₂²(10) motif.

BLYP/cc-pVDZ computations for the cyclic dimer model for **4** and **5** found a singlet ground state with a singlet–triplet splitting of $2J/k = -430$ J/mol, corresponding to $J \sim -26$ K ($\Delta E_{S-T} = 2J/k$). B3LYP/cc-pVDZ computations of the same type found $2J/k = -160$ J/mol, corresponding to $J \sim -10$ K. For these computations the GUESS = MIX keyword was used for the singlet states, in accord with recent trends in DFT treatments of biradical systems.^{20,21} The results support the throughspace exchange model in Chart 2 and are in accord with the overall finding of antiferromagnetic exchange. The small spin density on the –(N)–H atom of the benzimidazole (–0.2% at the BLYP/cc-pVDZ level of theory; see the Supporting Information) apparently is insufficient to provide a spin-polarization exchange pathway through the hydrogen bond in the dimer, which is required in order for ferromagnetic exchange to be observed.

While it is simplistic to model the behavior of the bulk solid by the cyclic dimer alone, the fact that the dimer is the only close approach of the interacting nitroxides makes it a reasonable model assemblage for computational study. BLYP/cc-pVDZ computations on a simplified model representing interaction between two molecules in a canted stack show the singlet and triplet states to be degenerate, consistent with the N–O···O–N

(18) (a) Aubrey, A.; Brembilla, A.; Fairve, V.; Lochon, F. *Acta Crystallogr. C* **1995**, *51*, 115. (b) Ohishi, H.; In, Y.; Ishida, T.; Inoue, M. *Acta Crystallogr. C* **1989**, *45*, 1921.

(19) See a detailed discussion with references in: Yamaguchi, K.; Kawakami, T.; Oda, A.; Yoshioka, Y. In *Magnetic Properties of Organic Materials*; Lahti, P. M., Ed.; Marcel Dekker: New York, 1999; Chapter 20, pp 403–426.

(20) Davidson, E. R. *Int. J. Quantum Chem.* **1998**, *69*, 241–245.

(21) Bally, T.; Borden, W. T. In *Reviews in Computational Chemistry*; Lipkowitz, K. B., Boyd, D. B., Eds.; John Wiley & Sons: New York, 1999; Vol. 13, pp 1–97.

not rule out such behavior in other systems. Still, it shows that hydrogen bonds can be seen solely as crystal engineering scaffolding rather than as invariably playing an electronic role in the design of molecular magnetic materials.

Experimental Section

General Procedures. All reagents were obtained from commercial suppliers and used without further purification. Tetrahydrofuran (THF) was distilled from sodium/benzophenone immediately prior to use. Glassware was dried in an oven and assembled under argon. Melting points were taken in Pyrex capillary tubes on an electrothermal apparatus and are uncorrected. ^1H NMR spectra were recorded on a Bruker AC-200 spectrometer in deuterated solvents. Chemical shifts are reported in parts per million. Infrared spectra were recorded on a Midac M-9000 spectrometer interfaced to a Pentium PC with Grams32 software (Galactic Industries Corp.). ESR spectra were obtained on degassed samples in 4 mm o.d. quartz tubes, using a Bruker ESP-300E spectrometer connected to an Aspect computer running standard Bruker interface software for spectral acquisition and workup. Elemental analyses were carried out at the University of Massachusetts Micro-analytical Laboratory.

5(6)-Chloro-1-(hydroxymethyl)benzimidazole. This compound was made by the method of Varma et al. to give a white, crystalline solid with mp 167–169 °C (lit. mp^{7a} 167–168 °C). ^1H NMR (200 MHz, DMSO- d_6): δ 8.3 (s, 1 H, imidazole 2-CH), 6.75–7.80 (m, 3 H, aryl H), 5.5 (d, 2 H, $-\text{CH}_2-$).

5,6-Dimethyl-1-(hydroxymethyl)benzimidazole. This compound was made by the method of Varma et al. to give a white, crystalline solid with mp 195–197 °C (lit.^{7b} mp 197–200 °C). ^1H NMR (200 MHz, DMSO- d_6): δ 8.03 (s, 1 H, 2 position on =CH), 7.39 (s, 2 H, aryl H), 5.5 (d, 2 H, $-\text{CH}_2-$), 2.35 (s, 3 H, $-\text{Me}$), 2.34 (s, 3 H, $-\text{Me}$).

2-(*N*-*tert*-butyl-*N*-hydroxylamino)-5(6)-chlorobenzimidazole (8). To a stirred solution of 0.24 g (1.56 mmol) of 5(6)-chloro-1-(hydroxymethyl)benzimidazole in 20 mL of THF was added to 2 mL of *n*-BuLi (1.6 M solution in hexane) at -75 °C. After the reaction was stirred at this temperature for 45 min, a solution of 0.26 g (3.0 mmol) of 2-methyl-2-nitrosopropane in 5 mL of THF was added by cannula. The reaction was stirred for 2 h and quenched with saturated aqueous ammonium chloride. The phases were separated, and the aqueous layer was extracted with ethyl ether. The combined organic layers were extracted with 2×50 mL of 0.1 N aqueous HCl. The combined aqueous layers were separated and neutralized with solid sodium bicarbonate. The resulting organic layer was extracted with ethyl ether and dried over anhydrous magnesium sulfate. After filtration, the solvent was removed under vacuum and the resultant crude solid immediately purified by flash chromatography (1:1 acetonitrile/benzene) to give 0.25 g (65%) of product as a white solid **8** with mp (dec) 161–163 °C. This material could be stored for a few days under argon in a freezer but generally was oxidized in the subsequent step as soon as was convenient. FTIR (KBr, cm^{-1}): 3433–2970 broad (OH plus NH str). ^1H NMR (200 MHz, DMSO- d_6): δ 11.6 (s, 1 H broad, N–H), 9.6 (s, 1 H, OH), 6.98–7.25 (3 H, aryl H), 1.37 (s, 9 H, *tert*-butyl).

2-(*N*-*tert*-butyl-*N*-aminoxyl)-5(6)-chlorobenzimidazole (4). To a suspension of 0.05 g (0.2 mmol) of **8** in chloroform was added 0.5 g (2.0 mmol) of lead dioxide. The mixture was stirred for 3 h, filtered, and concentrated under vacuum. The residual solid was redissolved in pentane, and insoluble

impurities were separated by centrifugation. The clear, red pentane solution was slowly evaporated under argon to give 0.016 g (37%, mp 112–114 °C) of **4** as red platelets. FTIR (KBr, cm^{-1}): 3298 (sharp, NH str), 2931–3000 (weak C–H str). ESR ($\nu_0 = 9.800412$ GHz, modulation frequency = 100 kHz, modulation amplitude = 0.37 G, benzene): $a_N = 10.01, 2.12,$ and 0.44 G; $a_H = 0.85, 0.78, 0.59,$ and 0.45 G. Elem anal. Calcd for $\text{C}_{11}\text{H}_{13}\text{ClN}_3\text{O}$: C, 55.35; H, 5.49; N, 17.60. Found: C, 55.64; H, 5.71; N, 16.68.

2-(*N*-*tert*-butyl-*N*-hydroxylamino)-5,6-dimethylbenzimidazole (9). To a suspension of 1.05 g (4.5 mmol) of 5,6-dimethyl-1-(hydroxymethyl)benzimidazole in 20 mL of dry THF were added 7.5 mL of *n*-BuLi (1.6 M solution in hexane) at -75 °C. The reaction was stirred for about 2 h and then cooled to -75 °C again before adding a solution of 0.6 g (7.2 mmol) of 2-methyl-2-nitrosopropane in 5 mL of THF. The reaction was reacted for 3 h and quenched with ammonium chloride (saturated solution in water). The phases were separated, and the aqueous layer was extracted several times with ethyl ether. The combined organic phases were then extracted with 0.1 N aqueous HCl. The combined aqueous layers were neutralized with solid sodium bicarbonate, extracted with ethyl ether, dried over anhydrous magnesium sulfate, filtered, and concentrated. The oily crude material was recrystallized from ethyl ether/pentane to yield 1.0 g (71%) of **9** as a white solid [mp (dec) 177–179 °C]. FT-IR (KBr, cm^{-1}): 3234 (OH str), 2983 (CH str). ^1H NMR (200 MHz, acetone- d_6): δ 8.6 (s, 1 H), 7.06 (s, 1 H), 7.14 (s, 1 H), 2.25 (s, 6 H), 1.41 (s, 9 H).

2-(*N*-*tert*-butyl-*N*-aminoxyl)-5,6-dimethylbenzimidazole (5). A total of 0.48 g (2.06 mmol) of **9** was suspended in 1:1 acetonitrile/benzene, and then 1.0 g (4.2 mmol) of lead oxide was added and the reaction stirred for 4 h. The solvent was removed and residue immediately purified by passing through a column of silica gel using a 1:1 ethyl ether/hexane mixture as the solvent. The red band was eluted and allowed to evaporate slowly in a beaker to yield 0.05 g [10%, mp (dec) 117–120 °C] of **5** as red crystals. FTIR (KBr, cm^{-1}): 3304 (sharp, NH str), 2963 (CH, str). ESR ($\nu_0 = 9.6367$ GHz, modulation frequency = 100 kHz, modulation amplitude = 0.3 G, benzene): $a_N = 10.25, 2.19,$ and 0.37 G; $a_H = 0.19, 0.39, 0.45, 0.48, 0.49, 0.53, 1.15, 1.30,$ and 1.31 G (fit by WINSIM⁹ has correlation 0.963). Elem anal. Calcd for $\text{C}_{13}\text{H}_{18}\text{N}_3\text{O}$: C, 67.21; H, 7.81; N, 18.09. Found: C, 67.37; H, 8.01; N, 17.30.

Acknowledgment. This work was supported by the National Science Foundation (CHE 9809548) and the Comision Interministerial de Ciencia y Tecnologia (CICYT-MAT97-0951). The opinions expressed in this paper are solely those of the authors and not necessarily those of the Foundation. We also acknowledge assistance from the Naval Research Laboratory for assistance with crystallographic analysis. CIF files for all crystal structures described in this paper may be obtained over the Internet at <http://www.chem.umass.edu/~lahti/xray>.

Supporting Information Available: Includes details of crystallographic and magnetic susceptibility analysis, tables of crystallographic data and CIF files for **4** and **5**, FTIR and ESR spectra for **4** and **5**, FTIR spectrum for **3** (N–D), and archival data from dimer model computations (PDF). See any current masthead page for ordering and Internet access information.

CM010322H